Fang, L.; Yan, W.; Noechel, U.; Kratz, K.; Lendlein, A.:

Programming structural functions in phase-segregated polymers by implementing a defined thermomechanical history

In: Polymer (2016) Elsevier

DOI: 10.1016/j.polymer.2016.08.105

Programming Structural Functions in Phase-segregated Polymers by Implementing a Defined Thermomechanical History

Liang Fang[a,#], Wan Yan[a,b], Ulrich Nöchel[a], Karl Kratz[a], and Andreas Lendlein[a,b,c]*

[a] Institute of Biomaterial Science and Berlin-Brandenburg Center for Regenerative Therapies, Helmholtz-Zentrum Geesthacht, Kantstr. 55, 14513, Teltow, Germany

[b] Institute of Chemistry, University of Potsdam, 14476 Potsdam, Germany

[c] Tianjin University–Helmholtz-Zentrum Geesthacht, Joint Laboratory for Biomaterials and Regenerative Medicine, Kantstr. 55, 14513 Teltow

[#] Present address: State Key Laboratory of Materials-Oriented Chemical Engineering, College of Material Science and Engineering, Nanjing Tech University, 210009, Nanjing, China.

*Corresponding author: Prof. Andreas Lendlein, Institute of Biomaterial Science and Berlin-Brandenburg Center for Regenerative Therapies, Helmholtz-Zentrum Geesthacht, Kantstr. 55, 14513 Teltow, Germany

Phone: +49 3328 352 450; Email: andreas.lendlein@hzg.de.

Keywords: Temperature-memory effect, Phase morphology, Thermomechanical history

Abstract

Unwanted shrinkage behaviors or failure in structural functions such as mechanical strength or deformability of polymeric products related to their thermomechanical history are a major challenge in production of plastics. Here, we address the question whether we can turn this challenge into an opportunity by creating defined thermomechanical histories in polymers, represented by a specific morphology and nanostructure, to equip polymeric shaped bodies with desired functions, e.g. a temperature-memory, by hot, warm or cold deformation into multiblock copolymers having two partially overlapping melting transitions. A copolyesterurethane named PDLCL, consisting of poly(*ε*-caprolactone) (PCL) and poly(*ω*-pentadecalactone) (PPDL) crystalline domains, exhibiting a pronounced phase-segregated morphology and partially overlapping melting transitions was selected for this study. Different types of PCL and PPDL crystals as well as distinct degrees of orientation in both amorphous and crystalline domains were obtained after deformation at 20 or 40 °C and to a lower extent at 60 °C. The generated non-isotropic structures were stable at ambient temperature and represent the different stresses stored. Stress-free heating experiments showed that the relaxation in both amorphous and crystalline phases occurred predominantly with melting of PCL crystals. When the switching temperature, which was similar to the applied deformation temperature (temperature-memory), was exceeded in stress-free heating experiments, the implemented thermomechanical history could be reversed. In contrast, during constant-strain heating to 60 °C the generated structural features remained almost unchanged.

These findings provide insights about the structure function relation in multiblock copolymers with two crystalline phases exhibiting a temperature-memory effect by implementation of specific thermomechanical histories, which might be a general principle for tailoring other functions like mechanical strength or deformability in polymers.

1. Introdcution

The complex thermomechanical history of plastics originating from their production and processing often creates challenges such as unwanted shrinkage behaviors or failure in structural functions of polymeric products [1-3]. Therefore, the knowledge about the thermal history of polymers is of great relevance [4-8]. The question that arises in this context is whether the implementation of a targeted thermomechanical history into polymeric materials can be advantageous for controlling specific functions of plastics? This might be possible when one understands how the morphology of a processed polymeric material is influenced by a specific thermomechanical treatment. In this regard, e.g. phase-segregated polymers are of great interest, because external thermomechanical stresses of the material can be transferred to or stored in different domains at micro and nano levels. Since polymer processing is typically performed in a small temperature window, it is of particular interest to utilize materials with multiple domains having different thermal transitions in a similar temperature interval.

One example for such materials are multiblock copolymers (MBCs) having a phase-segregated morphology presenting versatile systems of thermo-sensitive polymer networks, which are capable to memorize their original shape [9-13] or the temperature where the temporary shape was created during hot, warm or cold deformation [14-19]. Here, the temporary shape is stabilized by solidified switching domains associated to a glass (T_g) or melting transition (T_m). In polymer networks possessing a broad thermal transition [14, 15, 18, 19] or MBCs having two partially overlapping melting transitions [16], the switching temperature, where the original shape is recalled under stress-free conditions, can be controlled by variation of the deformation temperature. In this context, hot programming represents the deformation at temperatures above the thermal transition of the switching domains (T_{trans}), whereas during warm and cold programming the polymer is deformed at temperatures within or below T_{trans} [17]. While in covalently crosslinked polymer networks chemical netpoints are determining the original shape, in MBCs physical netpoints associated

to hard domains take this function. MBCs with two partially overlapping melting transitions are capable to precisely remember whether they have been deformed under cold, warm or hot conditions when they were heated again. So far, not much is known about the underlying mechanism how the information about the deformation temperature or the related thermomechanical history is stored within these polymer materials. Consequently, the nanostructural changes in the crystalline netpoints occurring during deformation at hot, warm or cold conditions need to be considered besides the alteration of the switching domains' crystal structure for understanding the relation between structure and property i.e. the temperature-memory capability.

In the current study, we explored whether a specific thermomechanical history can be implemented by hot, warm or cold deformation of multiblock copolymers having partially overlapping melting transitions resulting in specific morphologies and nanostructures, which are representative for the memorized deformation temperature. For this purpose, a copolyesterurethane named PDLCL, consisting of poly(ε-caprolactone) (PCL) crystalline domains as switching domains and poly(ω-pentadecalactone) (PPDL) crystalline domains as netpoints was chosen [16]. The selected PDLCL material solution cast thin films of PDLCL had an amount of 60 wt% PCL diol in the starting mixture of the oligomeric diols. The copolyesterurethane exhibited a pronounced phase-segregated morphology characterized by two distinct, partially overlapping melting transitions while a single glass transition has been reported indicating a mixed amorphous phase. Differential scanning calorimetry (DSC), wide- and small-angle X-ray scattering (WAXS, SAXS) and atomic force microscopy (AFM) experiments were conducted for investigating the thermal properties, crystal orientation and size as well as the surface morphologies of PDLCL before and after implementation of the specific thermomechanical histories. Finally, the nano-structural changes related to the temperature-memory capability of the differently treated PDLCL samples during stress-free or constant-strain heating was investigated by AFM, WAXS and SAXS.

2. Experimental

2.1 Materials

The copolyesterurethane PDLCL was synthesized by reaction of PPDL-diol with M_n = 4400 g•mol^{-1}, PCL-diol with M_n = 3000 g•mol^{-1} and 1,6-hexamethylene diisocyanate as reported previously in Ref. [16]. The prepared PDLCL had a PCL diol weight content of 60 wt% in the starting mixture of the oligomeric diols and exhibited a number average molecular weight of M_n = 99000 g•mol^{-1} and the polydispersity index was 5.1 as determined by multi detector gel permeation chromatography.

2.2 Film preparation

The solution cast thin PDLCL films were prepared from a chloroform solution with a polymer concentration of 0.3 wt%, resulting in PDLCL films with a thickness of 20±1 μm.

2.3 Characterization methods

2.3.1 *Differential Scanning Calorimetry*

DSC experiments were carried on a DSC 204 Phoenix (Netzsch, Selb, Germany) at a heating rate of 10 K•min^{-1} in sealed aluminum pans. The polymer samples were cooled from room temperature to 0 ºC before heating to 120 ºC. The melting temperatures (T_m) and the related melting enthalpies were determined from the first heating runs. Furthermore, the weight percent crystallinity (W_c) of PCL and PPDL segments was calculated from DSC curves using equation (1), where, ΔH_m is the melting enthalpy, representing the area of the melting peak. The ΔH_m^{100} is the specific melting enthalpy for a 100% crystalline PCL or PPDL segment, which were chosen as 135 [20] and 227 J•g^{-1} [21], respectively. Due to the overlap of PCL and PPDL melting peaks, the lowest point located in the overlapping area was chosen to separate the two melting peaks. The experimental errors were estimated: for measured T_m ±1 ^{o}C and for ΔH_m ±2 J•g^{-1}.

$$w_c = \frac{\Delta H_m}{\Delta H_m^{100}} \cdot 100 \quad (1)$$

2.3.2 *Deformation procedures*

Deformation of PDLCL samples was performed with test specimen type 1BB (EN ISO 527-2/1BB) using a tensile tester Z 1.0 (Zwick, Ulm, Germany) equipped with a thermo chamber and a temperature controller (Eurotherm Regler, Limburg, Germany). The specimens were maintained at different deformation temperatures (T_{deform}s) of 20 °C or 40 °C or 60 °C for 10 min and afterwards deformed to an elongation of ε_m = 100% at 10 mm•min^{-1}, where the strain was kept constant for 5 min to allow relaxation. Subsequently, the specimens were cooled to 0 ºC at 5 °C•min^{-1} and equilibrated for 10 min before releasing the stress.

2.3.3 *Atomic Force Microscopy*

The PDLCL films were investigated by AFM with a MFP-3D AFM (Asylum Research, Santa Barbara, CA, USA). The scan rate was 1.5 Hz and the mode was non-contact. The temperature was controlled by an environmental controller (Asylum Research, Santa Barbara, CA, USA) with a Peltier element. Silicon cantilevers (Olympus OMCL AC200TS-R3, Japan), having a driving frequency of around 150 kHz and a spring constant of 9 N•m^{-1} were used. The applied heating rate was 20 K•min^{-1}. Before scanning, the samples were equilibrated at the chosen temperature for 5 min. For scanning the surface morphologies of the specimens during the constant-strain recovery, the central area of the deformed specimens was cut off and attached to a sticky carbon tape (Plano GmbH, Wetzlar, Germany). A custom-made holder was utilized for scanning the surface morphologies of the specimens during the stress-free recovery. In this holder the specimens were fixed at both ends for AFM investigation, while during step-wise heating only one end of the test sample remained fixed allowing temperature-induced shape changes.

2.3.4 *Wide and small angle X-ray scattering*

The non-deformed samples were measured at 25 and 70 °C, while the programmed samples which already fixed at 0 °C were measured at 20, 40 and 60 °C by increasing the temperature gradually. Both WAXS and SAXS measurements at different temperatures were conducted according to the methods described in Ref. [22].

2.3.5 *Wide angle X-ray scattering*

WAXS measurements were performed on a D8 Discover X-ray diffraction system with a two-dimensional detector (1024×1024 pixel) from Bruker AXS (Karlsruhe, Germany). The X-ray generator was operated at 40 kV and 40 mA on a copper-anode. The collimator was 0.8 mm (beam size). The distance sample-detector was 150 mm, calibrated with corundum standard and the wavelength λ = 0.15418 nm. Exposure time was 300 s per scattering pattern. The raw 2D-patterns integrated to obtain 1D-scattering curves using 5-point normalized binning. Non-valid data points outward of the detector were not considered for integration. The scattering curves of semi-crystalline samples were decomposed into individual peaks, belonging either to the amorphous or the crystalline phase with the Bruker-software TOPAS®. An amorphous bump was always present at $2\theta \sim 20°$, crystalline peaks were found at various positions. The peaks of the two phases (amorphous and crystalline) were fitted with Pearson VII functions. The relation of the peak position and width (FWHM) with the crystal size (D_{110}) is given by the Sherrer equation (Equation (2)) (parameter k = 0.9).

$$D_{110} = \frac{k*\lambda}{B*cos\theta} \quad (2)$$

Where, B = FWHM (in radians); θ = half scattering angle; λ = wavelength of X-rays. The experimental error for measured D_{110} was estimated to be ±0.2 nm.

2.3.6 *Small angle X-ray scattering*

SAXS was performed on a Nanostar diffractometer (Bruker AXS, Karlsruhe, Germany), operating 40 kV and 35 mA on a copper anode. Point focussed X-rays were monochromated and parallelized by Montel-optics and collimated by a 750/400/1000 µm 3-pinhole

combination, thus a 400 μm beam having a wavelength of 0.15418 nm (CuKα) was obtained. The distance sample to detector was 1070 mm calibrated with Silver behenate standard. A Vantec-2000 detector (2048×2048 pixel, 68 μm pixel size) was employed to record scattered intensities. The primary and secondary beam paths as well as the sample chamber were operated under vacuum (~10^{-3} mbar).

Samples were placed into a Peltier heating/cooling stage and exposed for 3 h to obtain a two dimensional scattering pattern which was corrected for spatial distortion and background subtracted (weighted with sample transmission). Isotropic scattering patterns were integrated (azimuthal average over 360°) by 5-point binning with a 0.01° (2θ) step size from $2\theta = 0.1°$ to 3.2° leading into one-dimensional curves of scattered intensity *vs*. scattering angle (*I vs*. 2θ). Anisotropic scattering patterns were integrated over a 10° wide azimuthal range along the axis of symmetry (fiber axis, s_3). Furthermore, scattering angle was converted into scattering vector s, being $|s| = s = (2/\lambda) \sin\theta$ and a Kratky-plot (Lorenz correction Is^2 *vs*. *s*) was utilized to extract the long period *L* from the position of the peak maxima as $L = s^{-1}$. The experimental error for measured *L* was estimated to be both ±0.2 nm. The crystalline and amorphous layer thickness (d_c and d_a) were determined from the interface distribution functions (IDF), which were calculated from the SAXS intensity profile according to ref. [23]. The lower value of *d* obtained from IDF the selected as d_c since W_c were < 50%.

3. Results and Discussion

In the current study, the influence of a specific thermomechanical history obtained by hot, warm or cold deformation on the resulting crystalline nanostructure of the copolyesterurethane PDLCL as well as the nanostructural changes occurring during stress-free and constant strain heating was explored.

The scheme in Fig. 1a illustrates the hypothesis for the crystalline structures (PPDL crystals are orange and PCL crystals are blue) in PDLCL at different temperatures before deformation, after deformation and subsequent cooling. Before applying deformation, all non-oriented PCL crystals were present in the sample at 20 °C as 20 °C < $T_{m,onset,PCL}$. At 40

°C, some extent of the crystal population was in the amorphous state and only thermally stable (large) PCL crystals remain in the sample. When the temperature increased to 60 °C, all PCL crystals were changed to the molten state at 60 °C, while PPDL crystals in samples did not melt. After the cold drawing at 20 ºC and subsequent fixation, highly oriented PCL and PPDL crystals were obtained with smaller sizes due to the high degree of fragmentation of previous crystals. When T_{deform} was 60 ºC, new PCL crystals were generated by thermally-induced crystallization during cooling, presenting the lowest degree of orientation and the largest crystal size. The deformation at 40 °C and cooling resulted in the mixture of different types of PCL crystals and intermediate degree of orientation.

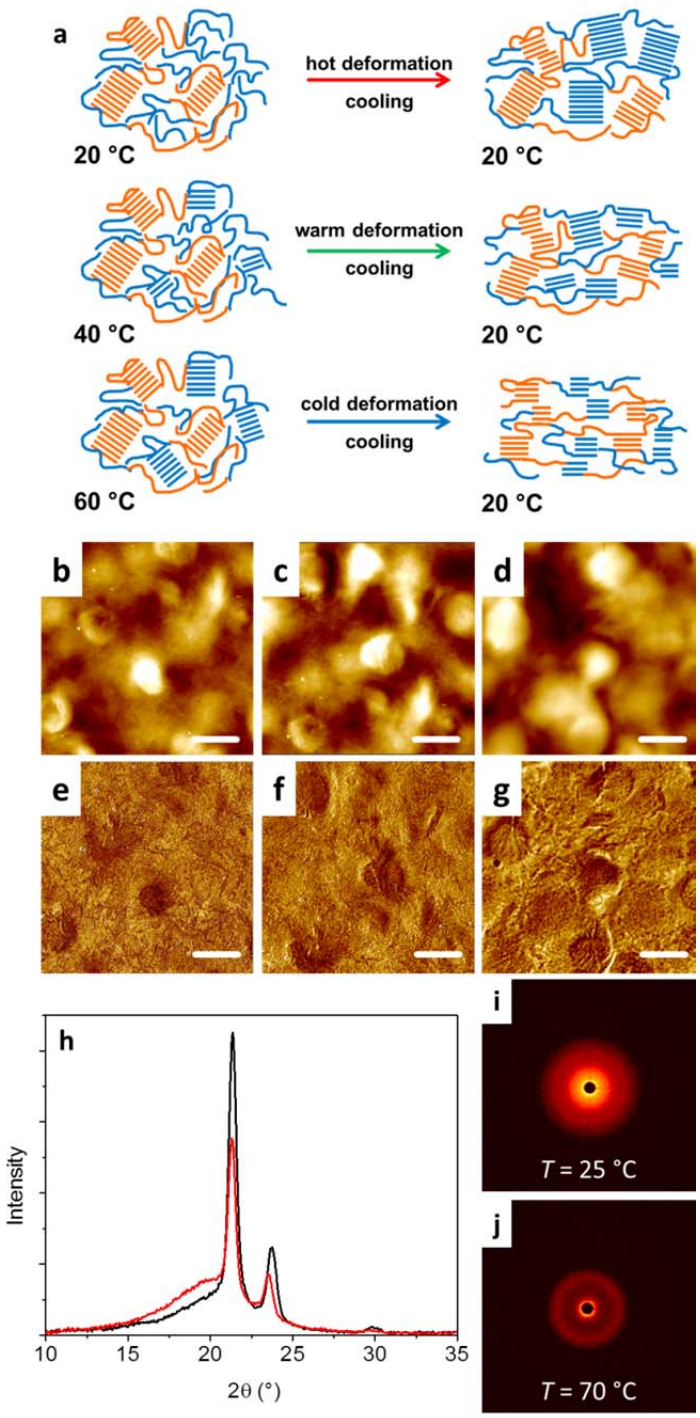

Fig. 1. (a) Schematic representation of the evolution of different crystalline structures in PDLCL (orange: PPDL crystals, blue: PCL crystals) obtained by hot (60 °C) or warm (40 °C) deformation and subsequent cooling to 20 °C or after cold deformation (20 °C). AFM height (b-d) and phase (e-g) images of as-cast, original PDLCL films scanned at three different temperatures, i.e. (b, e) 20 ºC, (c, f) 40 ºC, and (d, g) 60 ºC. The scale bar presents 2 μm. Deformation direction is vertical. 2D WAXS profiles of original PDLCL films (h) at 25 °C (black line) and 70 ºC (red line). 2D SAXS pattern of PDLCL films at 25 °C (i) and 70 ºC (j).

3.1. Characteristics of as-cast, original films

At first, the thermal properties as well as the morphology and the crystal structure of the as-cast PDLCL films were investigated by means of DSC, AFM, WAXS and SAXS experiments. The obtained results are summarized in Table 1. The DSC heating thermogram revealed a melting transition related to the PPDL crystals with a peak maximum at $T_{m,\,PPDL}$ = 83±1 °C and a melting transition interval $\Delta T_{m,\,PPDL}$ = 22±1 °C. The melting transition of PCL crystals, starting from $T_{m,\,onset,\,PCL}$ = 32±1 °C, also covered a wide temperature range of $\Delta T_{m,\,PCL}$ = 33±1 °C. The peak maximum was located at $T_{m,\,PCL}$ = 54±1 °C. Such wide range of the separated $T_{m,\,PPDL}$ and $T_{m,\,PCL}$ indicated well segregated PCL and PPDL crystalline domains. However, an overlap of the two melting transitions was observed at the temperature range between 60 and 75 °C. The W_c was calculated based on the melting enthalpy obtained from DSC curves and shown in Table 1. The weight percent crystallinity (W_c) of PCL and PPDL segments was calculated according to equation (1). Here, $W_{c,\,PCL}$ was 31±1%, while $W_{c,\,PPDL}$ was found at 46±1%. On the basis of the obtained thermal properties for PDLCL, 20, 40, and 60 °C were selected as T_{deform} for creating specific thermomechanical histories via cold, warm and hot deformation. These three different temperatures will lead to distinct structures and quantities of PCL and PPDL crystals before deformation as illustrated in Fig. 1a. All non-orientated PCL crystals were present at 20 °C. These PCL crystals partially melt to amorphous chains at 40 °C and all PCL crystals changed to molten state at 60 °C.

Table 1. Starting point of PCL melting transition ($T_{m,\,onset,\,PCL}$), weight crystallinity (W_c), long period (L), average lateral crystal size (D_{110}) and full width at half maximum ($FWHM$) of PDLCL films before and after deformation at 20, 40 and 60 ºC, determined or calculated based on DSC, SAXS and WAXS results.

	original	T_{deform}		
		20 ºC	40 ºC	60 ºC
$T_{m,\,onset,\,PCL}$[a] [ºC]	32±1	35±1	42±1	48±1
$W_{c,\,PCL}$[a] [%]	31±1	32±1	28±1	20±1
$W_{c,\,PPDL}$[a] [%]	46±1	48±1	51±1	55±1

L^b [nm]	13.3±0.2 (25 ºC)	14.4±0.2 (70 ºC)	10.7±0.2 (20 ºC)	13.2±0.2 (20 ºC)	14.9±0.2 (20 ºC)
D_{110} [nm]	16.9±0.2 (25 ºC)	17.3±0.2 (70 ºC)	9.9±0.2 (25 ºC)	12.6±0.2 (25 ºC)	16.3±0.2 (25 ºC)
$FWHM^d$ [º]	-	-	12.1±0.2	20.7±0.2	25.3±0.2

[a] $T_{m,\,onset}$ and w_c were calculated from DSC results. The estimated errors were: T: ±1 °C and W_c: ±1%.
[b] L was calculated from SAXS results with an estimated error of ±0.2 nm.
[c] D_{110} was calculated from WAXS data with an estimated error of ±0.2 nm.
[d] $FWHM$ was calculated based on azimuthal plots using Gaussian function with an estimated error of ±0.2°.

The surface morphologies of as-cast PDLCL films were characterized using AFM in a non-contact mode. The obtained AFM height and phase images are presented in Fig. 1b-g. The scanning temperatures were 20, 40, and 60 ºC, identical to the selected T_{deform}s, to evaluate temperature related morphological changes. At 20 ºC crystals with spherical structure protruding from the polymer matrix were observed with diameters around 1-3 µm (Fig. 1b and 1e). The crystals could consist of fibrils, which radiated outward from the center, forming the round shape. Both images illustrated that before deformation, both amorphous and crystalline phases in PDLCL exhibited no orientation. When increasing the temperature to 40 ºC (Fig. 1c, f), lower quantities of crystal structures were observed because of the partial melting of PCL crystals, while both amorphous and crystalline domains remained almost isotropic. At 60 ºC, which was close to the offset of $T_{m,\,PCL}$, a lower number of crystals (mainly PPDL crystals) was observed (Fig. 1d, g).

WAXS was performed to study the crystal structures of original PDLCL thin films. As shown in Fig. 1h, two main diffraction peaks located at 21.4º and 23.8º were observed, which are related to the (110) and (200) crystallographic planes of both, PCL and PPDL crystals [24, 25], crystallizing almost isomorphic and thus exhibiting overlapping reflections. By increasing the temperature to 70 °C, only PPDL crystalline reflections were expected and the resulting scattering curve had increased amorphous character. The average lateral crystal size

D_{110} = 16.9±0.2 nm determined at 25 °C was contributed by both PCL and PPDL crystals. At 70 °C, an increased D_{110} = 17.3±0.2 nm was determined, which was only related to the PPDL crystals as PCL was expected to be amorphous. SAXS measurements exhibited circular correlation rings at both 25 °C and 70 °C (Fig. 1i, j), which were related to the isotropic state of the crystalline domains, indicating that the crystals had no preferred orientation, which matched the AFM results. The long period as a measure for the distance between crystalline lamellae, including a crystalline and amorphous part, was determined from the scattering curve after Lorentz correction. At 25 °C L = 13.3±0.2 nm was contributed by both PCL and PPDL phases. Increasing the temperature to 70 ºC, where all PCL crystals are molten, resulted in L = 14.4±0.2 nm and can be solely attributed to the PPDL phase.

3.2 Characteristics of deformed films having defined thermomechanical histories

The thermal properties of PDLCL films deformed at different temperature were studied by DSC and the obtained data are summarized in Table 1. As shown in Fig. 2a, when deformed at 20 ºC, the peak location of $T_{m,\,PPDL}$ did not show considerable variation in comparison to the DSC curve of the original PDLCL film. The $T_{m,\,onset,\,PCL}$, however, shifted from 32 to 35 ºC and the W_c of both PPDL and PCL domains in the PDLCL film were slightly higher than those before deformation with $W_{c,\,PCL}$ = 32±1% and $W_{c,\,PPDL}$ = 48±1%. When T_{deform} = 40 ºC was applied, the $T_{m,\,onset,\,PCL}$ was shifted from 35 to 42 ºC. Increasing T_{deform} resulted in a reduction in $W_{c,\,PCL}$ to 28±1% while $W_{c,\,PPDL}$ increased from to 51±1%. Finally, at T_{deform} = 60 ºC, $W_{c,\,PCL}$ was found to be further decreased to 20±1%, while $W_{c,\,PPDL}$ was increased again to 55±1%. When deformed at 60 °C the PCL crystals in PDLCL films started to melt at a relatively high $T_{m,\,onset,\,PCL}$ of 48 ºC.

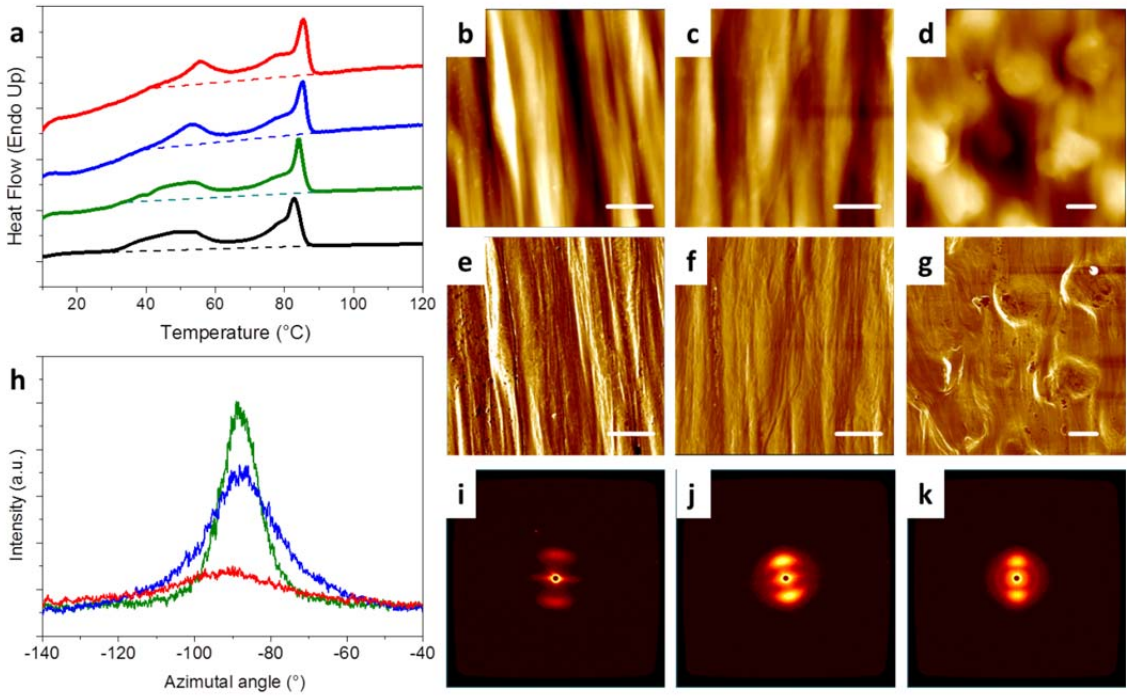

Fig. 2. (a) DSC thermograms (first heating run) of original PDLCL film (black line) and films deformed at different T_{deform} of 20 °C (blue), 40 °C (green) and 60 °C (red). The dotted line represents the baseline utilized for analysis. The curves were shifted vertically for better clarity. AFM height (b-d) and phase (e-g) images of PDLCL films deformed at different T_{deform}s scanned at 30 ºC. The scale bar presents 2 µm and the deformation direction is vertical. (h) Azimuthal intensity profiles of the crystalline (110)-reflection obtained from WAXS for T_{deform}; 20 °C (blue), 40 °C (green) and 60 °C (red). The curves were shifted vertically for better clarity. 2D SAXS patterns of films deformed at different T_{deform}s (i-k) .The colored frames represent hot, (red: T_{deform} = 60 °C) warm (green: T_{deform} = 40 °C) and cold (blue: T_{deform} = 20 °C) deformation procedure.

AFM images of the deformed PDLCL films with T_{deform} of 20, 40, or 60 ºC were taken at 30 °C and are displayed in Fig. 2b-g. The AFM height and phase images of a PDLCL film exposed to cold deformation (T_{deform} = 20 ºC) are shown in Fig. 2b, e. Here, both amorphous and crystalline phases were highly oriented, while no spherical structure of crystals can be observed in contrast to the initial morphology presented in Fig. 1. Similar results were observed in previous investigations reporting that the spherical structure of semi-crystalline polymers undergo fragmentation during stretching [26, 27]. Here, the homogenous spherical structure disappeared, while lamella fragments oriented along the stretching direction were

generated. When deformed at 40 ºC (Fig. 2c, f), the PDLCL film exhibited an oriented surface morphology along the stretching direction. When the deformation was performed at 60 ºC, the resulting morphology was substantially different from those obtained at lower T_{deform}s. Some spherical structures could be observed, although the oriented morphologies were still evident in the remaining regions (Fig. 2d, g). This result indicated that at T_{deform} = 60 ºC not all polymeric structures can be oriented.

WAXS measurements were performed to obtain a view of the oriented crystals in PDLCL thin films after deformation. The corresponding azimuthal profiles for the PDLCL samples programmed at different T_{deform}s are displayed in Fig. 2h. The azimuthal angle at around –90º refers to the equatorial axis (perpendicular to the drawing direction). Here, perpendicular crystal orientation refers to the interchain direction as the equatorial (110) reflections were used for analysis, consequently the molecular chains would be oriented parallel to the drawing direction. 2D scattering patterns of the lower-angle WAXS regime are presented in supplementary Fig. S1. As can be observed, there seems to be a very weak reflection appearing on the meridian when the sample was deformed at 20 °C, which was attributed to a PPDL (001) signal. Nonetheless, signal intensity after integration was too weak for analysis. The sharpness of the profile as a measure for the degree of orientation of the (110) crystal plane increased with decreasing T_{deform}, which was attributed to increased alignment of polymer chains along the drawing direction with higher remaining crystallinity. The full width at half maximum (FWHM) of the peaks in azimuthal plots were calculated based on Gaussian function, which increased from 25.28^{o} to 20.67^{o} and 12.10^{o} when T_{deform} decreased from 60 to 40 and 20 ^{o}C. The average lateral crystal size (D_{110}) was also affected by T_{deform} applied during deformation as the results listed in Table 1 illustrate. For T_{deform} = 20 °C, D_{110} was reduced from 16.9±0.1 (as-castd, original) to 9.9±0.1 nm after cold deformation, which was attributed to significant fragmentation of the existing crystals. For T_{deform} = 40 °C this effect was also existent but less pronounced indicated by D_{110} = 12.6±0.1 nm. After application of the hot deformation protocol (T_{deform} = 60 °C) an D_{110} of 17.0±0.2 nm was found, which was close to the dimension before deformation and can be attributed to a

predominant recrystallization of PCL domains during cooling. These findings could also be correlated to the SAXS pattern in Fig. 2i-k recorded after deformation. Here, the pattern became anisotropic presenting scattering maxima on the meridian (parallel to the drawing direction), which were attributed to stacks of crystalline-amorphous layers oriented perpendicular to the deformation direction. Furthermore, the scattering maxima had a dot-like shape, when T_{deform} = 60 °C was used, related to the laterally extended character of the lamellae. In contrast, the deformation at T_{deform} = 20 °C resulted in a more streak-like character of the scattering maxima, which is characteristic for laterally less extended structures. The long period was reduced after deformation at lower T_{deform} to values of 14.9±0.2 nm for 60 °C, 13.2±0.2 nm for 40 °C, and 10.7±0.2 nm for 20 °C. These results are in good agreement to the observations from WAXS related to crystal fragmentation at lower T_{deform}. Similar conclusion can be also obtained from the changes in d_c and d_a by computing the IDF. The d_c in deformed samples increased from 4.7±0.2 nm to 6.0±0.2 nm with increasing T_{deform}, indicating that larger crystals formed after higher temperature deformation.

Based on the obtained characteristics for deformed PDLCL films the mechanisms behind the structure evolutions during cold, warm and hot deformation are discussed in the following. At T_{deform} = 20 ºC, most PCL crystals still existed in PDLCL films before deformation. During the stretching, the PCL and PPDL amorphous phases were oriented along the strain direction. The crystal fragmentation, which took place during the deformation, resulted in multiple new physical netpoints, which restricted the relaxation of the amorphous chains after releasing the stress and a high degree of orientation remained in the deformed samples. The highly oriented amorphous phase could also facilitate the strain-induced crystallization, while the shortest chains with the highest orientation might provide the nucleation points. The high degree of fragmentation of previous PCL and PPDL crystals lead to the reduction in the average lateral crystal size and long period [28-31]. These newly generated crystal lamellae were highly oriented and perpendicular to the stretching directions (Fig. 1a), as indicated by WAXS and SAXS. Here, perpendicular crystal orientation refers to the interchain direction as the equatorial (110) reflections were used for

analysis, consequently the molecular chains would be oriented parallel to the drawing direction. Furthermore, the strain-induced crystallization may compensate the fragmentation of the previously existing crystals during the cold deformation and thereby resulted in a similar $W_{c,\ PCL}$ compared to the original sample. When T_{deform} = 40 ºC was applied, the remaining PCL round crystals with $T_{m,\ PCL}$ > 40 ºC and the PPDL crystals became fragmented lamellae. The average lateral crystal size and long period thus were reduced. During the equilibration step the oriented polymer chains now possessed tendencies to relax, decreasing the extent of orientation in amorphous phases. Subsequent cooling resulted in thermally-induced crystallization of PCL segments. Since a reduction in $W_{c,\ PCL}$ was observed, the newly created PCL crystals obtained from strain-induced and thermally-induced crystallization could not compensate the disappearance of the PCL crystals due to the melting and fragmentation. In addition, the orientation degree of the crystals was reduced at T_{deform} of 40 ºC because of the rearrangement of crystalline phases resulting from the relaxation of amorphous phase as well as the contribution of thermally-induced crystallization. As the selected T_{deform} of 60 ºC (hot deformation) was close to the upper limit point of the $T_{m,\ PCL}$, most PCL crystals were molten at this temperature. The drawing of the PDLCL film, thus, mostly led to the orientation of only PPDL lamellae, as well as the alignment of PCL and PPDL amorphous phases. During equilibration at 60 °C, after deformation was completed, the oriented PCL and PPDL chains in the amorphous phases relaxed extensively generating spherical structures. While reducing the temperature to 0 ºC, the resulting PCL crystals were mainly contributed by the thermally-induced crystallization. These newly created crystals possessed a low orientation degree and $W_{c,\ PCL}$. The possible strain-induced crystallization of PPDL segments and the smallest level of destruction in previous PPDL lamellae caused a considerable increase in $W_{c,\ PPDL}$. In summary, the structures of PCL and PPDL amorphous and crystalline phases in the programmed PDLCL samples were highly dependent on T_{deform}.

3.3 Morphological and nanostructural changes during heating

The structural changes in PDLCL films with different thermomechanical histories during heating under stress-free and constant strain conditions were assessed by AFM, SAXS, and WAXS experiments performed by step-wise heating including an equilibration period after each temperature increase.

Fig. 3a-l show the AFM height images of the surface morphologies of PDLCL thin films deformed at different T_{deform}s taken during heating at 30, 40, 50 and 60 ºC in stress-free heating experiments, where the deformed samples were allowed to recover towards its original dimensions. For all samples the degree of orientation in the surface morphologies decreased with increasing heating temperature. For cold deformed samples (T_{deform} = 20 ºC) the initially highly oriented structure became gradually less oriented with increasing the temperature (Fig. 3a-d). A similar gradual relaxation behavior with raising temperature was observed for samples deformed at T_{deform} = 40 ºC, whereby some spherical structures became evident in the surface morphologies at temperatures ≥ 50 °C (Fig. 3g, h), contributed by the relaxation of the amorphous phases along with the melting of PCL crystals. Due to the existence of spherical structures in the surface morphology of PDLCL deformed at 60 ºC, the relaxations of structures upon heating was not clearly visible from the AFM images in Fig. 3i-l. In contrast, the AFM images obtained from heating experiments under constant strain conditions displayed in Fig. 3m-x, documented that the surface morphologies remained almost unchanged with increasing the temperature of investigation from 30 °C to 60 °C due to the external force from the sample holder.

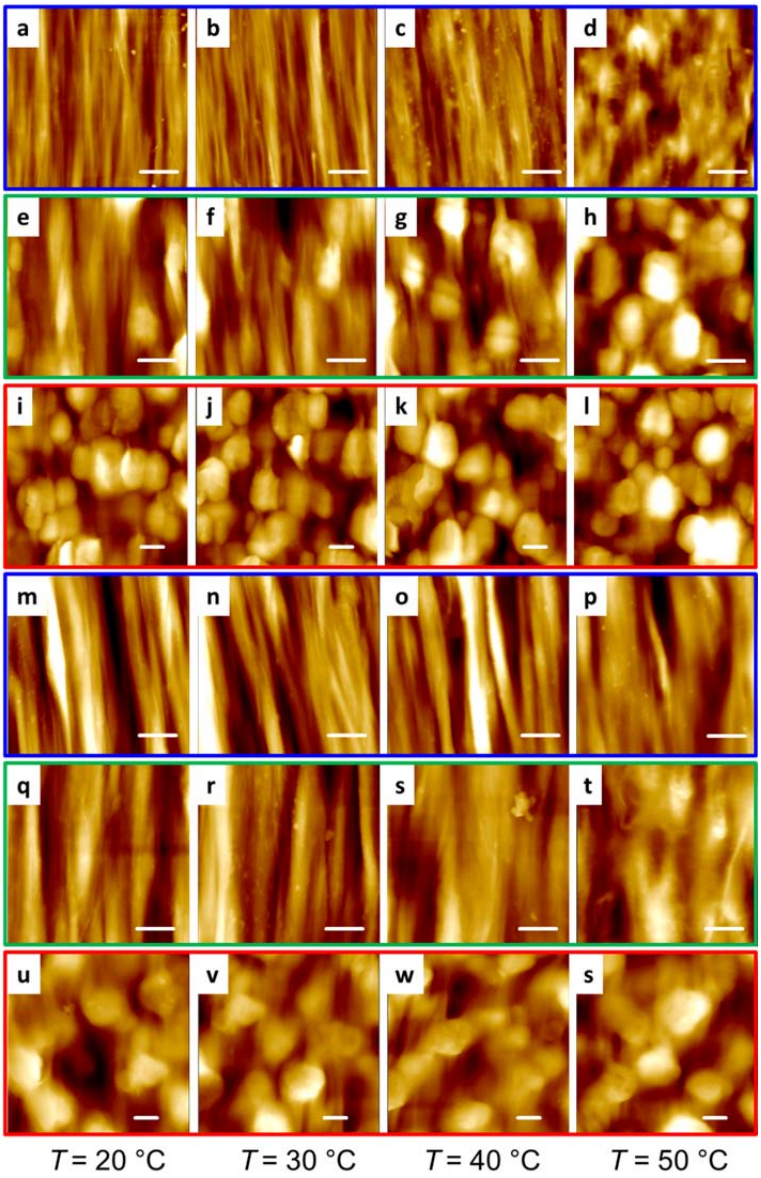

Fig. 3. AFM height images of PDLCL films deformed at different T_{deform} and subsequently reheated obtained under stress-free (a-l) and constant strain conditions (m-x) to scanning temperatures of 30 °C, (a, e, i, m, q, u) 40 °C (b, f, j, n, r, v), 50 °C (c, g, k, o, s, w) and 60 ºC (d, h, l, p, t, x). The scale bar presents 2 µm, the deformation direction is vertical and the colored frames represent hot, (red: T_{deform} = 60 °C) warm (green: T_{deform} = 40 °C) and cold (blue: T_{deform} = 20 °C) deformation procedure.

The heating induced changes in crystal structures and orientation of deformed PDLCL films were examined by WAXS and SAXS measurements. The azimuthal profiles obtained in stress-free heating WAXS experiments are shown in Fig. 4a-c, while the Kratky plots from SAXS intensity profile were presented in Fig. 5a-i. The determined lateral crystal sizes (D_{110}),

crystal thickness (d_a and d_c) and long periods (L) are listed in Table 2. For the cold programmed sample the peak intensity distribution of the azimuthal profiles (Fig. 4a) was reduced by increasing the temperature from 20 to 40 ºC. A more evident reduction in the intensity was observed when the temperature was increased to 60 ºC, which can be attributed to a melting of the majority of PCL crystals at this temperature. The FWHM correspondingly increased from 14.09^o to 30.08^o, indicating the decrease in the degree of orientation of crystal structures. Anyhow, at 60 °C there are still a few PCL as well as PPDL crystals presenting, which are oriented along the stretching direction. Similar results were observed in WAXS and SAXS patterns (Figs. S1 and S2), i.e. at 60 ºC the PPDL lamellae which were oriented perpendicular to the stretching directions resulted in the scattering maximum in equator. With increasing temperature the D_{110} and L were found to increase from D_{110} = 9.9±0.2 to 12.7±0.2 nm and L = 10.7±0.2 to 12.5±0.2 nm. The d_c also increased from 4.7±0.2 to 5.3±0.2 nm. These results indicated that the remaining PPDL lamellae possessed larger size and spacing than PCL crystals and confirmed that the cold deformation resulted in the fragmentation of PPDL crystals. When programmed at T_{deform} = 40 ºC a lower degree of the orientation becomes obvious from the azimuthal profiles taken at 20 °C shown in Fig. 4b, when compared to the cold programming scenario. Further increasing of the temperature to 60 ºC caused a significant increase in D_{110} from 12.6±0.2 nm to 15.4±0.2 nm. In contrast L remained almost unchanged. The d_c increased from 5.6±0.2 to 5.9±0.2 nm when the temperature increasing from 20 to 60 °C. For samples deformed at T_{deform} = 60 ºC WAXS and SAXS results indicated that the crystalline orientation completely disappeared upon heating to 60 °C, as demonstrated by the flat azimuthal intensity profile in Fig. 4c and the almost isotropic circular WAXS and SAXS pattern in Figs. S1 and S2. At 60 ºC PCL crystals are molten and most PPDL crystals presented no orientation. The obtained lateral crystal size as well as the long period were determined as D_{110} = 17.6±0.2 nm and L = 14.4±0.2 nm which were close to values obtained for the original non-deformed PDLCL film.

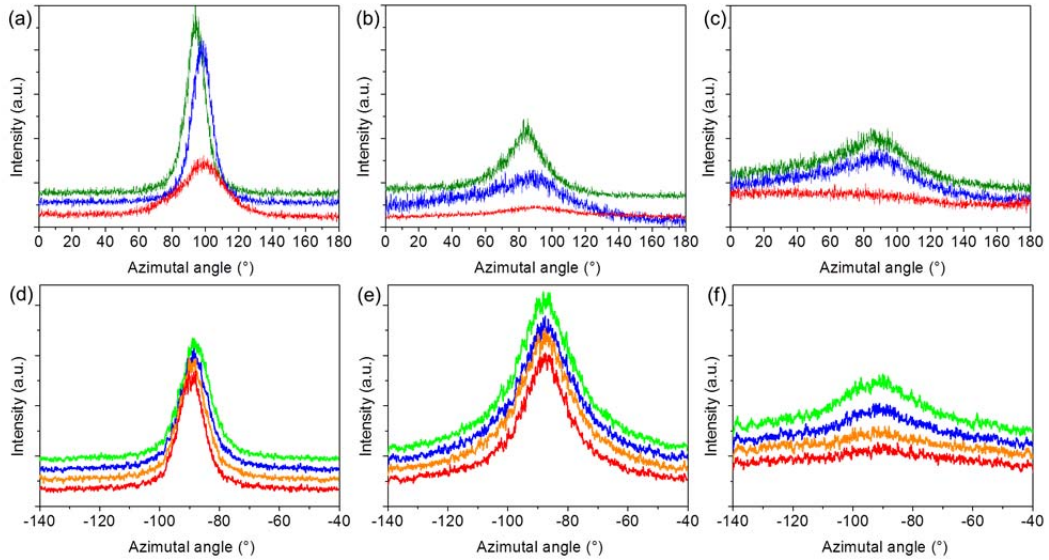

Fig. 4 Azimuthal intensity profiles of the crystalline (110)-reflection obtained from WAXS for PDLCL films deformed at different T_{deform} of 20 °C (a, d), 40 °C (b, e) and 60 °C (c, f) and subsequently reheated under stress-free (a-c) and constant strain conditions (d-f). The curves were shifted vertically for better clarity. The studied temperatures for stress-free experiments were 20 °C (blue), 40 °C (green), and 60 °C (red), while constant strain heating was investigated at 30 °C (cyan), 40 °C (green), 50 °C (orange) and 60 °C (red). The curves were shifted vertically for better clarity.

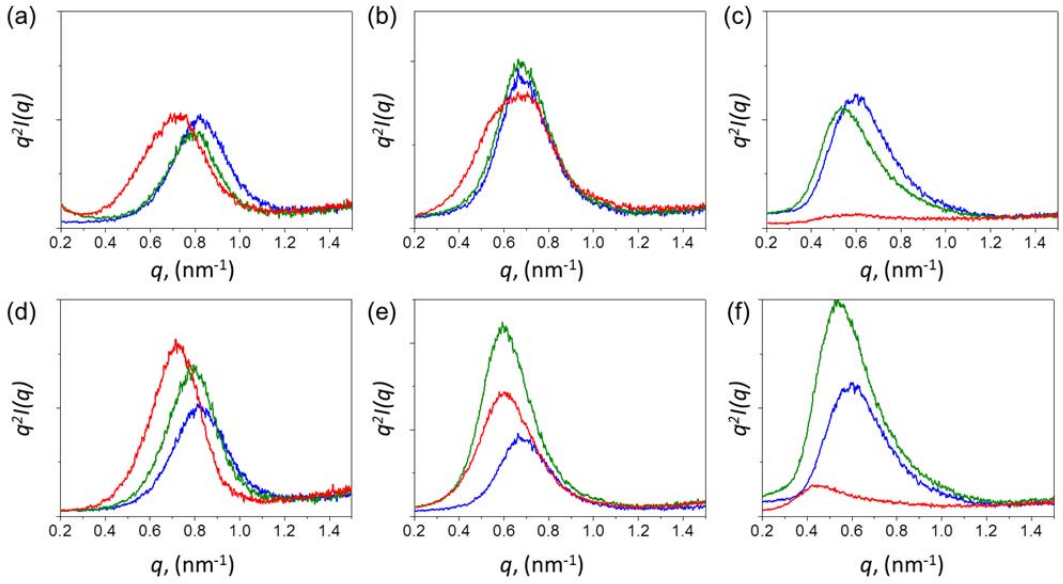

Fig. 5 Kratky plots from SAXS intensity profile of the PDLCL films deformed at T_{deform} of 20 °C (a, d), 40 °C (b, e) and 60 °C (c, f) and subsequently reheated under stress-free (a-c) and

constant strain conditions (d-f). The studied temperatures were 20 °C (blue), 40 °C (green), and 60 °C (red).

Table 2. Long period (L), average lateral crystal size (D_{110}) and full width at half maximum ($FWHM$) of PDLCL films obtained during heating under stress-free and constant strain conditions, calculated based on SAXS and WAXS results.

	T_{deform}		20 ºC	40 ºC	60 ºC
stress-free	20 ºC	L [nm]	10.7±0.2	11.2±0.2	12.5±0.2
		d_c+d_a [nm]	10.2±0.2	10.5±0.2	11.2±0.2
		d_c [nm]	4.7±0.2	4.8±0.2	5.3±0.2
		D_{110} [nm]	9.9±0.2	11.3±0.2	12.7±0.2
		$FWHM$ [^{o}]	14.1±0.2	14.7±0.2	30.1±0.2
	40 ºC	L [nm]	13.2±0.2	12.8±0.2	13.4±0.2
		d_c+d_a [nm]	11.4±0.2	11.6±0.2	11.8±0.2
		d_c [nm]	5.6±0.2	5.7±0.2	5.9±0.2
		D_{110} [nm]	12.6±0.2	12.5±0.2	15.4±0.2
		$FWHM$ [^{o}]	26.5±0.2	47.9±0.2	51.1±0.2
	60 ºC	L [nm]	14.9±0.2	15.6±0.2	14.4±0.2
		d_c+d_a [nm]	12.4±0.2	13.6±0.2	13.4±0.2
		d_c [nm]	6.0±0.2	6.4±0.2	3.8±0.2
		D_{110} [nm]	16.3±0.2	15.5±0.2	17.6±0.2
		$FWHM$ [^{o}]	37.6±0.2	47.9±0.2	N/A
constant-strain	20 ºC	L [nm]	10.7±0.2	11.2±0.2	12.3±0.2
		d_c+d_a [nm]	10.2±0.2	10.6±0.2	11.5±0.2
		d_c [nm]	4.7±0.2	5.0±0.2	5.9±0.2
		D_{110} [nm]	9.5±0.2	9.3±0.2	10.8±0.2

	FWHM [°]	12.0±0.2*	11.5±0.2	10.4±0.2
40 ºC	*L* [nm]	13.2±0.2	14.9±0.2	14.5±0.2
	d_c+d_a [nm]	11.4±0.2	13.0±0.2	12.8±0.2
	d_c [nm]	5.6±0.2	6.6±0.2	6.6±0.2
	D_{110} [nm]	12.3±0.2	12.2±0.2	13.2±0.2
	FWHM [°]	20.6±0.2*	20.3±0.2	18.0±0.2
60 ºC	*L* [nm]	14.9±0.2	15.6±0.2	19.8±0.2
	d_c+d_a [nm]	12.4±0.2	13.8±0.2	16.5±0.2
	d_c [nm]	6.0±0.2	6.4±0.2	5.0±0.2
	D_{110} [nm]	16.3±0.2	16.3±0.2	16.2±0.2
	FWHM [°]	26.2±0.2*	24.4±0.2	25.0±0.2

L was calculated from SAXS results with an estimated error of ±0.2 nm.
d_c and d_a were determined from interface distribution functions (IDF) calculated from SAXS profiles with an estimated error of ±0.2 nm.
D_{110} was calculated from WAXS data with an estimated error of ±0.2 nm.
* The FWHM data were calculated from azimuthal plot using Gaussian function with an estimated error of ±0.2 °.

When the heating of the deformed PDLCL samples was performed under constant strain the achieved azimuthal profiles (Fig. 4d-f) did not change considerably with increasing the temperature from 30 °C to 60 °C. As shown in Table 2, the calculated FWHM presents a negligible variation with temperature, which was different to the results obtained in stress-free heating experiments. These findings indicated that the crystal orientation could be maintained in the constant strain heating procedure for all deformed samples nearly independent from the applied T_{deform}, which is in good agreement with the AFM results shown in Fig. 3m-x. Here, the high degree of orientation achieved during cold (T_{deform} = 20 °C) or warm (T_{deform} = 40 °C) deformation of PDLCL was identical in the temperature range from 30 °C to 60 °C. Increasing in temperature from 20 °C to 60 °C caused melting of PCL crystals and similarly resulted in larger lateral crystal sizes and long periods, which were mainly attributed to PPDL

crystals (see Table 1). Likewise, the WAXS and SAXS patterns displayed in Figs. S1 and S2 did not change significantly during constant strain heating. These results demonstrated that heating at constant strain did not result in a significant variation in the orientation of both crystalline and amorphous domains generated by deformation at different temperatures. This might be related to the generation of internal intermolecular forces along the strain direction during constant strain heating as well as to the imposed external mechanical force, which restricted the mobility, and thereby limiting the relaxation of oriented polymer chains and melting of lamellae. Only in case of the hot deformed sample (T_{deform} = 60 °C) a continuous reduction in the degree of orientation during heating could be observed in azimuthal profiles (Fig. 4f). While the lateral crystal size was found to be constant around D_{110} = 16.3±0.2 nm the long period increased from L = 14.9±0.2 nm to L = 19.8±0.2 nm caused by the melting of PCL crystals. These findings might be attributed to regions of low degree of orientation present in samples deformed at T_{deform} = 60 °C, represented by the circular morphological features observed in AFM (Fig. 2d). In these regions the restrictions caused by intermolecular forces along the direction of deformation were weak and allowed relaxation of oriented crystalline and amorphous phases when the temperature is increased.

The results of shape-memory measurements under free-stress recovery were provided in the supporting information (Table S1). PCLDL film showed the lowest recovery ratio when the film was deformed at 20 °C, while the highest recovery ratio was obtained when the film was deformed at 40 °C. It can be explained by the observations in the structural variation of PCLDL samples. When the sample was deformed at 20 °C, highest level of crystal fragmentation including both PPCL and PCL crystals occurred, resulting in the crystals with smallest size. The reduction of netpoints (PPCL crystals) weakened its ability of shape-recovery. When the sample was deformed at high temperature of 60 °C, lowest degree of orientation was obtained after deformation, which also decreased the shape-recovery ratio. The change in switching temperatures is related to the T_ms of PCL crystals obtained after deformation at different temperatures, enabling the temperature-memory effect.

4. Conclusion

In the present study, it is shown that specific thermomechanical treatments of PDLCL multiblock copolymers with overlapping PCL and PPDL melting transitions via cold, warm or hot deformation resulted in pronounced differences in their crystalline nanostructures. After deformation, different types of PCL and PPDL crystals as well as distinct degrees of orientation in both amorphous and crystalline domains were obtained. Cold deformation leads to highest degree of orientation with small crystals by the fragmentation previous crystal lamellae. In contrast, when hot deformation was performed, thermally-induced crystallization of PCL domains during subsequent cooling was dominating the crystal structure resulting in a relatively low degree of orientation. During stress-free heating, the relaxation in both amorphous and crystalline phases occurred predominantly with melting of PCL crystals. PPDL crystals oriented perpendicular to the strain directions, which possessed smaller lateral crystal size and long period, were observed after heating to 60 °C for cold and warm deformed samples. In contrast, in constant-strain heating experiments the oriented structures generated during cold and warm deformation were almost remained. While in the hot deformed PDLCL, similar to the stress-free recovery, recoiling of the oriented amorphous and crystalline domains could be observed.

This research demonstrated that the implementation of specific thermomechanical histories in multiblock copolymers can be a powerful approach for tailoring the structural functions in polymers i.e. a temperature-memory effect, whereby the local thermomechanical stresses were stored in different domains at micro and nano level. In this way, the memorized deformation temperature can be related to a specific crystal structure. It is anticipated that the current findings are helpful for designing novel copolymers as well as adapted production processes suitable for implementing specific thermomechanical histories within a small processing temperature window suitable for adjusting plastics´ structural functions like mechanical strength or deformability.

Acknowledgements

The authors thank Dr. Michael Zierke for synthesis of copolyesterurethanes and Ms. Susanne Schwanz for technical support. This work was supported by the Helmholtz-Association through programme-oriented funding as well as through a fellowship for W.Y. by the Helmholtz Graduate School for Macromolecular Bioscience (VH-GS-503).

5. References

1. Ezrin M. Plastics Failure Guide. Plastics Failure Guide (Second Edition): Hanser, 2013. pp. I-XXXIV.
2. Jansen K.M.B., Van Dijk D.J., and Husselman M.H. Polymer Engineering & Science 1998;38(5):838-846.
3. Duoss E.B., Weisgraber T.H., Hearon K., Zhu C., Small W., Metz T.R., Vericella J.J., Barth H.D., Kuntz J.D., Maxwell R.S., Spadaccini C.M., and Wilson T.S. Advanced Functional Materials 2014;24(31):5020-5020.
4. Matsuoka S. Polymer Engineering & Science 1974;14(3):162-166.
5. Silva J., Meltzer D., Liu J., Cox M., and Maia J. Polymer Engineering & Science 2014;54(6):1383-1393.
6. Soong S.Y., Cohen R.E., Boyce M.C., and Chen W. Polymer 2008;49(6):1440-1443.
7. Miri V., Elkoun S., Peurton F., Vanmansart C., Lefebvre J.M., Krawczak P., and Seguela R. Macromolecules 2008;41(23):9234-9244.
8. Klompen E.T.J., Engels T.A.P., Govaert L.E., and Meijer H.E.H. Macromolecules 2005;38(16):6997-7008.
9. Fei P. and Cavicchi K.A. ACS Applied Materials & Interfaces 2010;2(10):2797-2803.
10. Feng Y., Behl M., Kelch S., and Lendlein A. Macromolecular Bioscience 2009;9(1):45-54.
11. Matsumoto H., Ishiguro T., Konosu Y., Minagawa M., Tanioka A., Richau K., Kratz K., and Lendlein A. European Polymer Journal 2012;48(11):1866-1874.
12. Kim B.K., Lee S.Y., and Xu M. Polymer 1996;37(26):5781-5793.
13. Momtaz M., Razavi-Nouri M., and Barikani M. Journal of Materials Science 2014;49(21):7575-7584.
14. Cui J., Kratz K., and Lendlein A. Smart Materials and Structures 2010;19(6):065019.

15. Kratz K., Madbouly S.A., Wagermaier W., and Lendlein A. Advanced Materials 2011;23(35):4058-4062.
16. Kratz K., Voigt U., and Lendlein A. Advanced Functional Materials 2012;22(14):3057-3065.
17. Li G. and Wang A. Journal of Polymer Science Part B: Polymer Physics 2016;54(14):1319–1339.
18. Miaudet P., Derré A., Maugey M., Zakri C., Piccione P.M., Inoubli R., and Poulin P. Science 2007;318(5854):1294-1296.
19. Xie T., Page K.A., and Eastman S.A. Advanced Functional Materials 2011;21(11):2057-2066.
20. Jiang S., Ji X., An L., and Jiang B. Polymer 2001;42(8):3901-3907.
21. Cai J., Hsiao B.S., and Gross R.A. Polymer International 2009;58(8):944-953.
22. Nöchel U., Reddy C.S., Wang K., Cui J., Zizak I., Behl M., Kratz K., and Lendlein A. Journal of Materials Chemistry A 2015;3(16):8284-8293.
23. W. Ruland. The evaluation of the small-angle scattering of lamellar two-phase systems by means of interface distribution functions. Colloid and Polymer Science, 1977;255(5):417–427.
24. H. Bittiger, R. H. Marchessault, and W. D. Niegisch. Crystal structure of poly(ε-caprolactone). *Acta Crystallographica Section B* 1970;26:1923–1927.
25. M. Gazzano, V. Malta, M. L. Focarete, M. Scandola, and R. A. Gross. Crystal structure of poly(ω-pentadecalactone). *Journal of Polymer Science Part B: Polymer Physics* 2003;41(10):1009–1013.
26. Thomas C., Seguela R., Detrez F., Miri V., and Vanmansart C. Polymer 2009;50(15):3714-3723.
27. Zia Q., Radusch H.-J., and Androsch R. Polymer bulletin 2009;63(5):755-771.
28. Kamal T., Shin T.J., and Park S.-Y. Macromolecules 2012;45(21):8752-8759.
29. Pople .J, Mitchell G., Sutton S., Vaughan A., and Chai C. Polymer 1999;40(10):2769-2777.
30. Xiong B., Lame O., Chenal J.-M., Rochas C., and Seguela R. Express Polymer Letters 2016;10(4): 311-323.
31. Yeh F., Hsiao B.S., Sauer B.B., Michel S., and Siesler H.W. Macromolecules 2003;36(6):1940-1954.